Efficiency of clay-TiO_2 nanocomposites on the photocatalytic elimination of a model hydrophobic air pollutant.

Daria Kibanova[1,2], Javiera Cervini-Silva [2,3] and Hugo Destaillats [4,5]

[1] Facultad de Química, Universidad Nacional Autónoma de México

[2] Instituto de Geografía, Universidad Nacional Autónoma de México

[3] NASA Astrobiology Institute

[4] Lawrence Berkeley National Laboratory,
Indoor Environment Department,
Environmental Energy Technologies Division

[5] Arizona State University,
Department of Civil, Environmental and Sustainable Engineering

January 2009

Experimental work was carried out at LBNL under US DOE Contract No. DE-AC02-05CH11231.This project was supported in part by LBNL (LDRD LB07014, Project # 366088), by UNAM (PAPIIT Grant No: IN116007-2) and by CONACYT (SEP-CONACYT Ciencia Básica 2006, Grant nr. 61670).

Efficiency of clay-TiO_2 nanocomposites on the photocatalytic elimination of a model hydrophobic air pollutant.

Daria Kibanova[1,2], Javiera Cervini-Silva [2,3,*] and Hugo Destaillats [4,5,*]

[1] Facultad de Química, Universidad Nacional Autónoma de México

[2] Instituto de Geografía, Universidad Nacional Autónoma de México

[3] NASA Astrobiology Institute

[4] Lawrence Berkeley National Laboratory,
Indoor Environment Department,
Environmental Energy Technologies Division

[5] Arizona State University,
Department of Civil, Environmental and Sustainable Engineering

*Corresponding address**:**

Hugo Destaillats
Lawrence Berkeley National Laboratory
1 Cyclotron Road, MS 70-108B
Berkeley, California 94720, USA
+1 (510) 486-5897
+1 (510) 486-7303 (fax),
HDestaillats@lbl.gov

Javiera Cervini-Silva
Universidad Nacional Autónoma de México
Circuito Exterior, Ciudad Universitaria
Coyoacán, C.P. 04150, México City, México
+52 (55) 5622-4336
+52 (55) 5616-2145 (fax),
jcervini@igg.unam.mx

Abstract

Clay-supported TiO_2 photocatalysts can potentially improve the performance of air treatment technologies *via* enhanced adsorption and reactivity of target volatile organic compounds (VOCs). In this study, a bench-top photocatalytic flow reactor was used to evaluate the efficiency of hectorite-TiO_2 and kaolinite-TiO_2, two novel composite materials synthesized in our laboratory. Toluene, a model hydrophobic VOC and a common indoor air pollutant, was introduced in the air stream at realistic concentrations, and reacted under UVA (λ_{max} = 365 nm) or UVC (λ_{max} = 254 nm) irradiation. The UVC lamp generated secondary emission at 185 nm, leading to the formation of ozone and other short-lived reactive species. Performance of clay-TiO_2 composites was compared with that of pure TiO_2 (Degussa P25), and with UV irradiation in the absence of photocatalyst under identical conditions. Films of clay-TiO_2 composites and of P25 were prepared by a dip-coating method on the surface of Raschig rings, which were placed inside the flow reactor. An upstream toluene concentration of ~170 ppbv was generated by diluting a constant flow of toluene vapor from a diffusion source with dry air, or with humid air at 10, 33 and 66 % relative humidity (RH). Toluene concentrations were determined by collecting Tenax-TA ® sorbent tubes downstream of the reactor, with subsequent thermal desorption – GC/MS analysis. The fraction of toluene removed, *%R*, and the reaction rate, T_r, were calculated for each experimental condition from the concentration changes measured with and without UV irradiation. Use of UVC light ($UV/TiO_2/O_3$) led to overall higher reactivity, which can be partially attributed to the contribution of gas phase reactions by short-lived radical species. When the reaction rate was normalized to the light irradiance, T_r/I_λ, the UV/TiO_2 reaction under UVA irradiation was more efficient for samples with a higher content of TiO_2 (P25 and Hecto-TiO_2), but not for Kao-TiO_2. In all cases, reaction rates peaked at 10% RH, with T_r values between 10 and 50% higher than those measured under dry air. However, a net inhibition was observed as RH increased to 33% and 66%, indicating that water molecules competed effectively with toluene for reactive surface sites and limited the overall photocatalytic conversion. Compared to P25, inhibition by co-adsorbed water was less significant for Kao-TiO_2 samples, but was more dramatic for Hecto-TiO_2 due to the high water uptake capacity of hectorite.

Keywords: 1:1 and 2:1 phyllosilicates, photocatalysis, indoor air quality, air cleaning, air contaminant, titania.

Introduction

Organic pollutants can be removed effectively from indoor air using active UV photocatalytic oxidation (UVPCO) methods *(1-4)*. Passive methods, in which volatile organic compounds (VOCs) react over irradiated indoor surfaces, have also been identified as promising pollution abatement technologies. For example, paint containing photocatalytic pigments was shown to catalyze the oxidation of indoor VOCs, although their efficiency still needs to be assessed *(5,6)*. The use of photoactive coatings in depolluting and self-cleaning external surfaces of buildings (such as glass windows, cement, etc) has also been extensively studied, and is currently being implemented in several commercial products *(3,7,8)*. In each of these applications, the photocatalytic particles –usually pure TiO_2- are supported on materials that must be strongly attached to building surfaces and/or to the air purifiers' hardware, resisting environmental aging and mechanical abrasion. Supports also should be chemically inert, or participate in the chemical process facilitating pollutant elimination. Other requirements for good photocatalyst supports include: 1) to facilitate mass transport to and from the active sites, 2) to increase the effective residence time in the proximity of the photocatalyst, and 3) to avoid blocking irradiation from the active sites. Support materials for TiO_2 include, among others, glass *(8-10)*, quartz *(11)*, paper *(12)*, cement *(7)*; activated carbon fibers *(13,14)*, ceramics *(15,16)*, stainless steel *(17)* and polymeric matrices such as poly(ethylene terephthalate) (PET) and cellulose acetate *(18,19)*. Similarly, significant research efforts have been made to improve the photocatalytic efficiency of TiO_2-based nanoparticles through chemical and physical transformations *(20-25)*. Such changes include doping with transition metal ions *(23)* and non-metallic elements *(24)*, as well as structural transformations at the nanometric scale such as the synthesis of *p-n* juncture nanotubes *(25)*.

Natural and synthetic clays are receiving increasing attention as supports of TiO_2-based photocatalysts for air and water remediation *(26-30)*. Clays present often a large surface area for reversible and irreversible adsorption of organic pollutants. Experimentally determined sorption rates indicate that significant amounts of VOCs adsorb onto internal clay surfaces, with inter-particle and intra-particle diffusional time constants spanning two orders of magnitude *(31)*. Embedding TiO_2 nanoparticles in clay matrices is expected to improve the photocatalytic performance by enhancing VOC

retention through adsorption in clay pores. In addition, clays can also act as electron acceptors or donors *(32)* and have the ability to catalyze diverse chemical processes such as polymerization, reduction, decomposition or acid-base reactions *(32-35)*. Synthesis of TiO_2 nanoparticles embedded in the structure of porous clays avoids the formation of macroscopic aggregates of photoactive particles that may lead to reduced efficiency. Furthermore, clays are stable supports that protect the TiO_2 particles from erosion or washing, and are inexpensive, non-toxic materials.

In the present study, we investigated the photocatalytic activity of two TiO_2-clay nanocomposite materials synthesized in our laboratory *(36)*. The nanocomposites were illuminated with either UVA (λ_{max} = 365 nm) or UVC (λ_{max} = 254 nm) radiation. The UVC lamp used in our study generated secondary emission at 185 nm, in addition to the principal line at 254 nm. Co-generation of ozone in UVPCO applications with irradiation at 185 + 254 nm was shown to increase VOC removal efficiency, as compared with irradiation at exclusively 254 nm, and with longwave frequency of 365 nm *(37,38)*. Similarly, a recent study showed higher toluene oxidation rates and mineralization for the combined oxidation process UV/TiO_2/O_3 as compared with UV/TiO_2 *(39)*. Irradiation of the TiO_2 surface in the presence of ozone was shown to have a positive effect on the regeneration of the photocatalyst, due to enhanced elimination of non-volatile, partially oxidized byproducts that remained adhered to the photocatalyst *(40)*. For this reason, the combined UV/TiO_2/O_3 process is considered effective in improving the overall VOC removal efficiency, minimizing the formation of harmful partially oxidized volatile species and extending the lifetime of the photocatalyst through elimination of non-volatile oxidation byproducts from its surface. In UVPCO indoor air cleaning applications, excess ozone generated in the UV/TiO_2/O_3 process should be removed from the air before being delivered to occupied spaces through irradiation with ozone-degrading UV light of 254 nm and/or placing an activated carbon bed downstream of the unit.

In several studies, reactions catalyzed by UV/TiO_2 and UV/TiO_2/O_3 have been performed in bench-scale experiments using gas-phase VOC concentrations that are between 1 and 3 orders of magnitude higher than those that could be typically encountered in a UVPCO air cleaning system, principally due to limitations of the analytical methods used in those experiments *(37-41)*. Recently, photocatalytic

performance with ppbv-level VOC concentrations has also been reported *(4,42)*. Here, we investigate the potential of these reactions at VOC concentrations that occur in buildings (in the low ppb range), by applying sampling and analytical techniques commonly used in indoor air quality characterization *(43)*. We also investigated the adjuvant effect of ozone and other active oxygen species at low concentrations (≤ 250 ppbv O_3), compared with the much higher values reported by other authors (e.g., 3-15 ppmv O_3) *(39)*.

The main purpose of the present study is to evaluate the performance of two composites synthesized in our laboratory based on hectorite (Hecto-TiO_2) and kaolinite (Kao-TiO_2), under UVA (UV/TiO_2-clay) and UVC irradiation (UV/TiO_2-clay/O_3). We compared the performance of the two composites with that of pure TiO_2 (Degussa P25) under identical experimental conditions. We also investigated the effect of relative humidity (RH) in the range 0-66 % on the photocatalytic process with UVC irradiation, as well as on the direct photolysis/ozonolysis (UV/O_3). The oxidation of toluene was followed as a probe reaction. Toluene was selected as a model hydrophobic indoor air pollutant for two reasons: it is a compound for which photocatalytic oxidation pathways have been studied extensively *(42,44-46)*, and it is one of the predominant VOCs in indoor environments *(47,48)*. This study is specifically focused on toluene, a model hydrophobic VOC, because of its high levels indoors, and relatively lower removal efficiency achieved by conventional UVPCO methods *(4)*. Our results will help assess potential benefits and challenges associated with the use of clay minerals as supports for TiO_2-based photocatalysts.

Experimental Section

Materials

Kaolinite ($Al_2Si_2O_5(OH)_4$; KGa-1b) from Washington County, Georgia, USA and hectorite ($Na_{0.4}Mg_{2.7}Li_{0.3}Si_4O_{10}(OH)_2$; SHCa-1) from San Bernardino County, California, USA, were obtained from the Source Clays Repository of the Clay Minerals Society (Washington, DC). The clays have been characterized in the literature *(49)*, and were used as received. Titanium tetraisopropoxide $Ti(OC_3H_7)_4$ (97%), was from

Sigma-Aldrich (Milwaukee, WI); absolute ethanol (≥ 98%) from Riedel-de Haen (Switzerland); hydrochloric acid (reagent grade, 37%) from Aldrich (Milwaukee, WI). TiO_2 (P25) was obtained from Degussa (Germany). Toluene of >99.5% purity from Sigma-Aldrich (Milwaukee, WI) was used as model reactant without further purification. All stock solutions were prepared using de-ionized water (Millipore, 17.6MΩ-cm). Glass Raschig rings of 5 mm O.D. and 5 mm length were from Ace Glass (Vineland, NJ).

Preparation of photocatalyst coatings

Clay-TiO_2 composites. Description of the synthesis and characterization of the TiO_2–clay nanocomposites has been previously reported *(36)*. Briefly, a clay-water suspension (1% w/w) was stirred for 2 hours. A TiO_2 sol-gel solution was prepared by mixing titanium tetraisopropoxide with hydrochloric acid, nanopure water and absolute ethanol. The concentration of $Ti(OC_3H_7)_4$ in the sol-gel solution (Solution A) was 0.4 M with a H_2O/ $Ti(OC_3H_7)_4$ molar ratio of 0.82, and a pH = 1.27. Absolute ethanol was used to dilute Solution A to a final $Ti(OC_3H_7)_4$ concentration of 0.05 M (Solution B). An aliquot of Solution B was added to a clay suspension and the TiO_2 content in the suspension was 70% w/w, stirred for 24 h, and centrifuged at 3,800 rpm for 10 minutes. Then, the solid phase was washed three times with nanopure water. The resulting TiO_2-clay composite was dispersed in a 1:1 water: ethanol solution and exposed to hydrothermal treatment in an autoclave at 180°C for 5 hours. The product was centrifuged once again at 3,800 rpm for 15 minutes, and resuspended in absolute ethanol (Solution C).

Preparation of catalyst-coated Raschig rings. Fifty Raschig glass rings were coated with each of the TiO_2-clay composite samples and fifty more were coated with P25. Before coating, the rings were initially sonicated for 5 minutes in acetone, for 5 more minutes in de-ionized water, and dried at 60 ºC for 1 h. Each ring was dip-coated for 5 seconds in suspensions containing a) Solution C corresponding to one of the two TiO_2-clay composites, or b) P25 suspended in ethanol. Coated rings were placed in an oven at 110 ºC for 5 hours to evaporate the solvent, and stored in ambient conditions prior to use.

The average mass of the photocatalytic material deposited in each ring was determined as follows:

$$m_f = \frac{(m_c - m_g)}{50} \qquad (1)$$

where m_f is the average mass of photocatalytic material per ring, m_c is the mass of 50 coated rings and m_g is the mass of the same 50 rings determined before coating. The average mass m_f, together with $m_{f\text{-}TiO2}$, the corresponding average mass of TiO_2 deposited on each ring, is reported in Table 1 together with the BET surface area and the average pore area corresponding to each photocatalyst.

TABLE 1. Preparation of photocatalyst-coated Raschig rings.

Material	m_f	TiO_2 content [a]	$m_{f\text{-}TiO2}$	BET surface area [a]	Average pore volume [a]
	(mg)	(%)	(mg)	($m^2 g^{-1}$)	($cm^3 g^{-1}$)
Hecto-TiO_2	1.03	60.8	0.626	140	0.457
Kao-TiO_2	0.367	2.9	0.0105	15.9	0.670
P25	0.762	100	0.762	60.7	0.308

[a] Kibanova et al., 2009 – Reference *(36)*

Photocatalytic reactor and experimental methods

Experiments were carried out in the photocatalytic flow reactor illustrated in Figure 1S (Supporting Information). It consisted of a cylindrical quartz tube containing seven coated Raschig rings, which were irradiated by a UV lamp placed parallel to the tube at a constant distance of 25 mm. Two different lamps were used: a UVA lamp with $\lambda_{max.}$= 365 nm and irradiance of I_{365} = 0.77 mW.cm^{-2} (UVP Model 90-0019-01), and a UVC lamp with $\lambda_{max.}$= 254 nm and secondary emission at 185 nm with an irradiance of I_{254} = 2.8 mW.cm^{-2} (UVP Model 90-0004-01). Both lamps were manufactured by UVP (Upland, California), and their irradiance at 25 mm from the source was determined with a UVP radiometer calibrated at 365 nm and 254 nm, respectively. The lamp and

quartz tube were housed in a metallic container provided with a shield covering a variable length of the lamp, which was used to regulate the amount of UV light used in the experiments. The shield position was adjusted to expose a lamp length equal to that of the quartz tube containing the Raschig rings. This experimental arrangement allowed us to identify the optimal reactor length leading to a measurable toluene removal. A constant air flow of 500 $mL \cdot min^{-1}$ was circulated through the reactor. Two mass airflow controllers were used in parallel to adjust the flow of "zero" quality air from a commercial cylinder (Airgas, California) with a precision better than 1%. One of the airflows was saturated with moisture using a water bubbler, and the relative flows adjusted to achieve the targeted relative humidity (RH). A constant flow of toluene vapor was generated from a diffusion vial (VICI Metronics, TX) placed in a thermostatic bath, operated at a flow of 3 $cm^3.min^{-1}$, leading to a concentration of ~170 ppbv after dilution at the reactor inlet.

Temperature and RH were measured at the reactor outlet in real time using a HOBO sensor (Onset Corp., MA). Ozone was monitored in real time with a photometric analyzer (Model 400, API) downstream from the reactor. Integrated toluene samples were collected at the reactor outlet using sorbent Tenax-TA ® tubes (Supelco Analytical, PA) over 5-minute periods to accumulate enough analyte for GC-MS analysis. Quantification of toluene samples was carried out by thermal desorption gas chromatography with mass selective detection (TD-GC/MS) following the standard TO-1 EPA method *(50)*. An Agilent GC/MS (Model 6890/5973) was operated in electron impact mode, and was interfaced with a thermal desorption inlet with autosampler (Gerstel, Germany). A calibration curve for toluene in the range 5 – 150 ng was developed from direct injections of diluted standard solutions in sorbent tubes using bromofluorobenzene as internal standard.

Experiments were carried out by irradiating all the catalyst materials (rings coated with P25, Hecto-TiO_2, Kao-TiO_2 and uncoated rings) with UV light (UVA or UVC) in the presence of toluene at 10% RH. Also, the influence of relative humidity was explored using UVC irradiation at 0, 10, 33 and 66 % RH. In each experiment, the diluted toluene flow was allowed to circulate through the reactor without UV illumination for at least 30 minutes, in order to reach equilibrium with the photocatalyst and other internal surfaces of the reactor. Considering the low toluene concentrations

used in this study, the expected coverage is at the sub-monolayer level. At the end of this initial period, toluene samples were collected sequentially at the reactor outlet to determine the initial concentration, $[Tol]_0$. Subsequently, the UV light was turned on, allowing for at least 30 minutes of equilibration. During that period, toluene concentration at the reactor outlet decreased to a lower value due to partial removal through photocatalytic oxidation. After 30 minutes, at least three samples of toluene were collected sequentially to determine the outlet concentration during steady-state irradiation conditions, $[Tol]_{SS}$. Finally, the UV lamp was turned off, allowing for a final 30-min equilibration period. At the end of this period, a new set of samples of toluene were collected at the reactor's outlet to verify that its concentration was restored to its initial value, $[Tol]_0$. Figure 2S (Supp. Info.) illustrates results from a typical experiment. Given the very short reactor residence time of ~0.015 min, a 30-minute waiting period before collecting samples (equivalent to ~2,000 air exchanges) was sufficient to reach a new steady-state condition in each case. Comparison of sequentially collected samples, under irradiation and in the dark, allowed us to verify that steady-state was achieved in each case.

Results and discussion

The toluene % removal (*%R*) in each experiment was calculated as

$$\%R = \left(1 - \frac{[Tol]_{SS}}{[Tol]_0}\right) \times 100 \qquad (2)$$

and the toluene removal rate, T_r, expressed in ng.min^{-1}, was calculated as follows:

$$T_r = f\left([Tol]_0 - [Tol]_{SS}\right) \qquad (3)$$

where f is the airflow rate (in mL.min^{-1}), and the toluene concentrations are expressed in ng.mL^{-1}. In Figure 1, *%R* results under UVA and UVC illumination at 10% RH and 21 ^{o}C are presented together with toluene removal rates normalized to the mass of photocatalyst (T_r/m_f), to the mass of TiO_2 present in the photocatalyst ($T_r/m_{f\text{-}TiO2}$) and to

the UV light irradiance (T_r/I_λ). The corresponding values of each of these parameters are presented in Table 1S (Supporting Information).

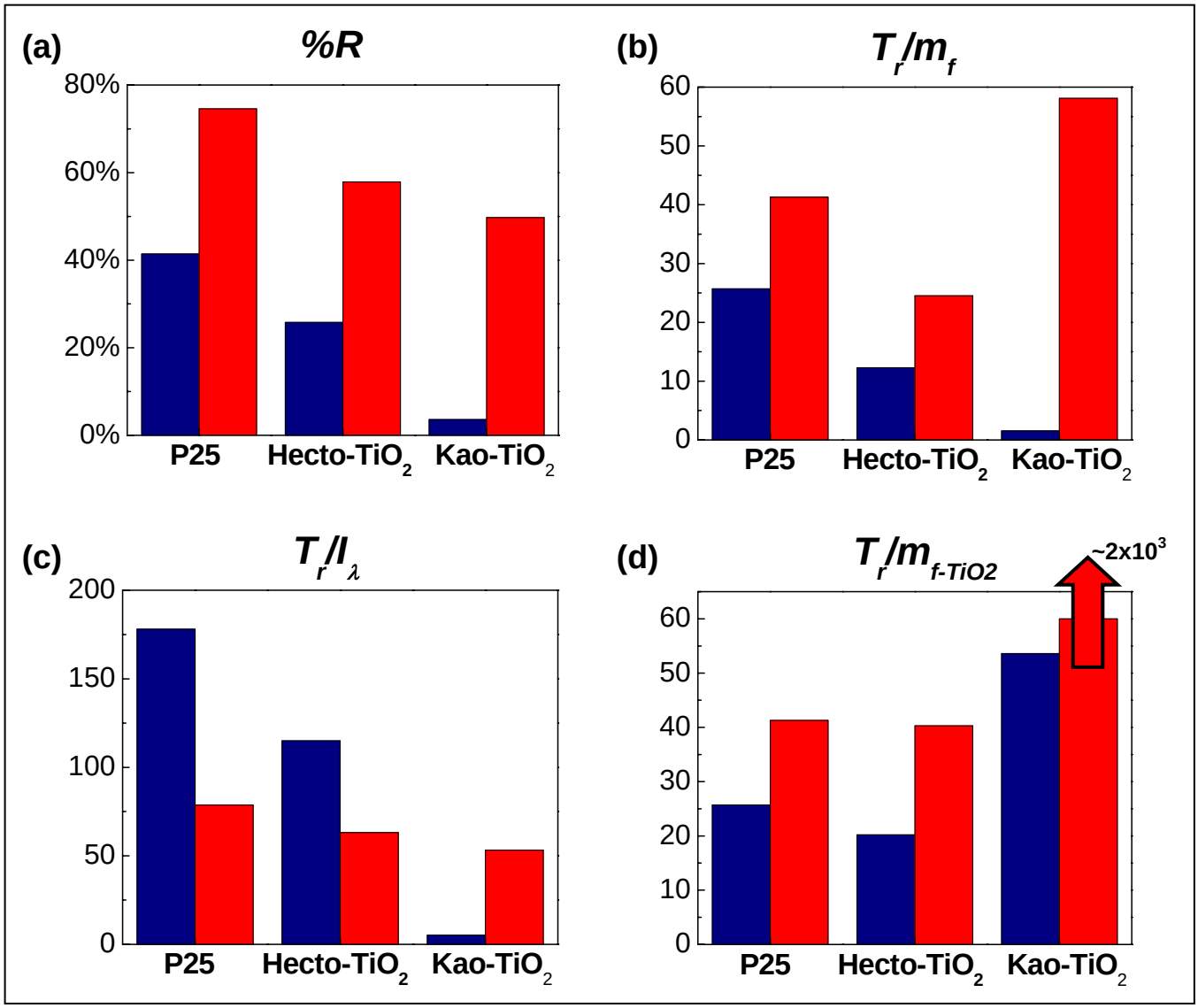

Figure 1: Experimental results under UVA (blue bars) and UVC (red bars) irradiation.

(a) Toluene % removal (*%R*);

(b) toluene removal rate normalized to the mass of photocatalyst T_r/m_f (in ng min^{-1} g^{-1});

(c) toluene removal rate normalized to the UV light irradiance T_r/I_λ (in ng cm^2 min^{-1} mW^{-1});

(d) toluene removal rate normalized to the mass of TiO_2 present in the photocatalyst $T_r/m_{f\text{-}TiO2}$ (in ng min^{-1} g^{-1}). Results are also listed in Table 1S (Supporting Information section).

Toluene removal under UVA

Toluene elimination rates were relatively high in the presence of P25 and Hecto-TiO_2 composites. In contrast, toluene removal by Kao-TiO_2 composites was modest. Oxidation rates T_r measured for the three photocatalysts were proportional to the relative TiO_2 content of each material, as shown in Figure 2, indicating that TiO_2 loading of the photocatalyst is the key parameter driving the photocatalytic process under UVA. Experiments using uncoated rings were also performed, in which no toluene degradation was observed under UVA illumination, and no formation of ozone was detected at the reactor outlet. Gas chromatograms of samples obtained during periods under UVA irradiation showed no benzaldehyde, nor any other byproduct of toluene oxidation.

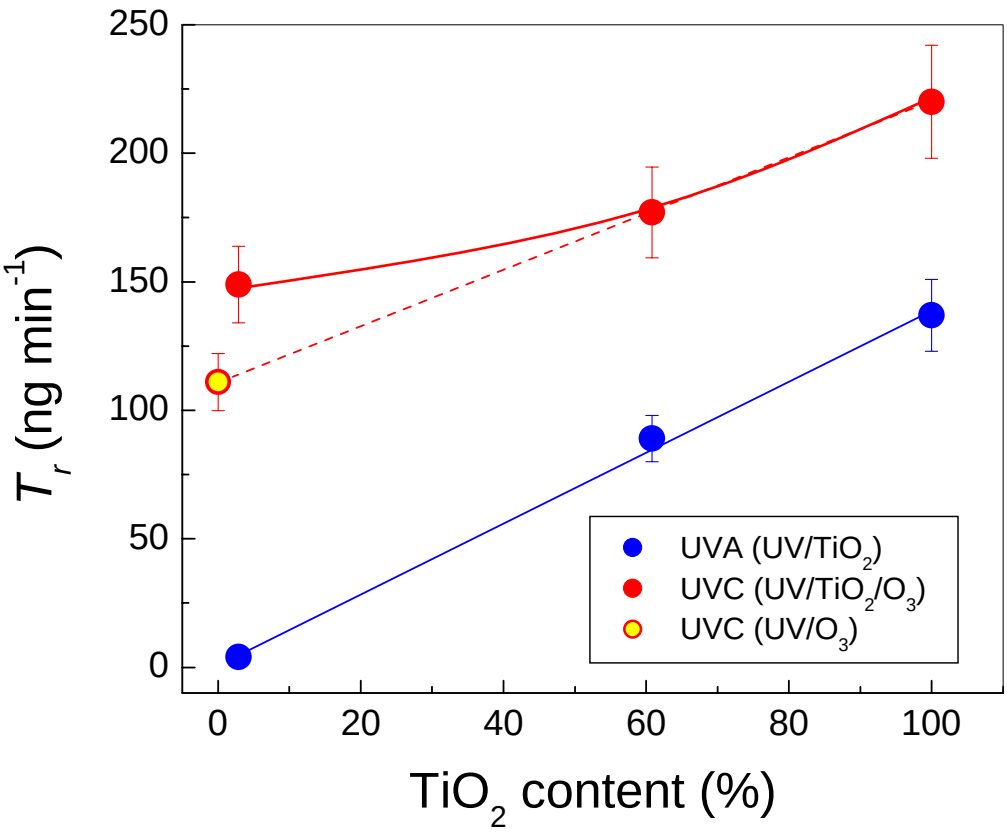

Figure 2: Toluene removal rate T_r as a function of TiO_2 content for P25 (100%), Hecto-TiO_2 (61%) and Kao-TiO_2 (3%).

Toluene removal under UVC

Irradiation with UVC light under identical flow conditions led to a significantly higher toluene elimination. However, after normalizing to the radiance of each lamp, the effective removal rates *Tr/I* reported in Table 1S and in Figure 1 are lower for the UVC lamp than for the UVA lamp, except for Kao-TiO_2. Figure 2 illustrates that toluene removal rates (T_r) for the two samples with higher TiO_2 content (P25 and Hecto-TiO_2) follow a trend parallel to that observed for the UVA lamp, which extrapolates at 0% TiO_2 to the T_r value measured with uncoated rings (i.e., UV/O_3). Under ozone-generating UVC irradiation (254 + 185 nm), T_r measured in the absence of photocatalyst (i.e., UV/O_3 oxidation) is relatively high. Ozone concentrations measured at the reactor outlet were in the range 100 – 250 ppbv. However, direct ozonation of toluene in the gas phase, with a bimolecular rate constant of $k^{tol}_{O3} = 9.9 \times 10^{-12}$ $ppbv^{-1}$ s^{-1} *(51)* is a slow reaction, and would not take place during the very short reactor residence time (~1 s). Instead, toluene reacted with short-lived species involved in ozone formation and degradation pathways. Ozone was formed by photochemical dissociation of O_2 molecules at 185 nm, as follows:

$$O_2 + h\nu\ (185\ nm) \rightarrow O(^1D) + O(^3P) \quad (4)$$

$$O(^1D) + O_2 \rightarrow O(^3P) + O_2 \quad (5)$$

$$O(^3P) + 2\ O_2 \rightarrow O_3 + O_2 \quad (6)$$

and decomposed by radiation of 254 nm:

$$O_3 + h\nu\ (254\ nm) \rightarrow O(^1D) + O_2 \quad (7)$$

The oxidation rate of toluene with $O(^3P)$ is fast, with a bimolecular rate constant of $k^{tol}_{O(3P)} = 2.1 \times 10^{-3}$ $ppbv^{-1}$ s^{-1} *(52)*. The lifetime of toluene due to this reaction is likely similar to the short reactor residence time. Hydroxyl radicals can be generated in the gas phase by reaction of water vapor with $O(^1D)$ atoms formed in the photolysis of O_2 and O_3:

$$O(^1D) + H_2O \rightarrow 2\ OH \quad (8)$$

and also by direct photolysis of water vapor

$$H_2O + h\nu\ (185\ nm) \rightarrow H + OH \quad (9)$$

Hydroxyl radicals can also react fast enough with toluene, having a bimolecular rate constant of $k^{tol}_{OH} = 0.16\ ppbv^{-1}\ s^{-1}$ *(53)*.

Figure 2 shows a significant positive deviation of T_r determined with the Kao-TiO_2 sample from the linear behavior predicted by the other two samples, indicating the presence of a large synergistic effect due to the combined presence of the photocatalyst, UV illumination and ozone (UV/TiO_2-clay/O_3). The higher-than-expected reactivity in the presence of Kao-TiO_2 surfaces could be explained by a) heterogeneous catalysis of toluene oxidation by gas phase reactive species generated in reactions 4-9, and b) the formation of other short-lived reactive species upon irradiation of the hydrated clay-TiO_2 composite surface. Gas chromatograms of samples obtained during periods under UVC irradiation showed no benzaldehyde, nor any other byproduct of toluene oxidation. This result, similar to that observed for UVA irradiation, suggests that partial oxidation byproducts likely include highly oxidized species, such as carboxylic acids, with low vapor pressures and a higher tendency to remain adsorbed to the photocatalyst or other internal reactor surfaces.

Effect of relative humidity on toluene removal

The effect of relative humidity (RH) on toluene removal under UVC irradiation was investigated using dry air, and humid air at 10%, 33% and 66% RH, to cover a broad ambient humidity range. In each case, experiments were performed using uncoated rings (UV/O_3), P25-coated rings (UV/TiO_2/O_3) and rings coated with Hecto-TiO_2 and Kao-TiO_2 composites (UV/TiO_2-clay/O_3). The values of T_r determined in each condition are presented in Table 2. In all cases, we observed a maximum toluene removal rate at RH = 10%, suggesting a positive effect of limited water coverage (i.e., less than a monolayer). This positive effect was counterbalanced by a larger negative effect observed at higher RH conditions, in which excess water competed with toluene molecules for reaction sites over the catalysts, in coincidence with previously reported

results *(54)*. Results presented in Table 2 indicate that water vapor plays a role not only on the heterogeneous photocatalytic process, but also on the homogeneous gas-phase chemistry under UVC irradiation, which also peaked at 10% RH. These results are consistent with previous observations of dramatic *(38)* and moderate *(55)* increases in gas phase reactivity of toluene under irradiation at (254+185) nm in the presence of water vapor *vis-à-vis* dry conditions.

TABLE 2. Effect of the relative humidity on the toluene removal rate T_r under UV/O_3, $UV/TiO_2/O_3$ and UV/TiO_2-clay/O_3.

Experimental conditions	*Tr* (ng.min^{-1})				Water loss at 300 °C (% of sample mass)
	RH = 0 %	RH = 10 %	RH = 33 %	RH = 66 %	
UV/Hecto-TiO_2/O_3	157 ± 11	177 ± 2	113 ± 9	102 ± 28	9.08 (6.96)[a]
UV/Kao-TiO_2/O_3	103 ± 3	149 ± 6	119 ± 16	86 ± 9	2.74 (0.98)[b]
UV/P25/O_3	196 ± 24	220 ± 9	183 ± 5	152 ± 3	1.72
UV/O_3	80 ± 16	111 ± 12	81 ± 26	61 ± 7	n.a.

[a] native hectorite
[b] native kaolinite

The direct photolysis/ozonolysis (UV/O_3) rate was significant for all RH conditions, but the toluene removal efficiency was improved in the presence of photocatalyst in all cases. Pure TiO_2 (P25) showed the highest overall toluene removal efficiency across the RH range. The two clay-TiO_2 samples showed intermediate performance, but Hecto-TiO_2 was more efficient than Kao-TiO_2. For each photocatalyst and for UV/O_3 reactions, the relative toluene removal rate T_r/T_r^0 (where T_r^0 is the toluene removal rate at 0% RH) is plotted in Figure 3. The ratio T_r/T_r^0 can be used to compare the relative enhancement ($T_r/T_r^0 > 1$) and inhibition ($T_r/T_r^0 < 1$) due to the presence of moisture. We observed that Kao-TiO_2 presented the highest enhancement at 10% RH and 33% RH, and only moderate inhibition at 66 % RH, with respect to values determined in dry air. Performance in UV/O_3 experiments was comparable to Kao-TiO_2, albeit with relatively higher inhibition by water. Given the overall low reactivity

observed for Kao-TiO_2, the RH effects observed with this photocatalyst can be mostly attributed to gas phase chemical processes (UV/O_3 reactions). Samples in which the photocatalytic process predominated (P25 and Hecto-TiO_2) showed a relatively smaller enhancement of T_r at 10% RH. At higher RH, Hecto-TiO_2 showed a particularly significant inhibition of T_r (with $T_r/T_r^0 < 0.7$ for 33% and 66% RH), indicating that water uptake by the clay competed favorably with the adsorption and photocatalytic elimination of toluene. This result coincides with high water contents of hectorite and of the Hecto-TiO_2 composite in equilibrium with air in ambient conditions, reported in Table 2 as mass loss upon heating at 300 °C. Incorporation of TiO_2 into hectorite led to a large reactive surface area, from which an important fraction corresponds to small-size pores of 1-30 nm *(36)*. The incorporation of water into those nanopores likely limited the photocatalytic reactivity of toluene, not only by competing for adsorption to photocatalytically active sites, but also by excluding the hydrophobic pollutant from the interior areas of the smaller pores.

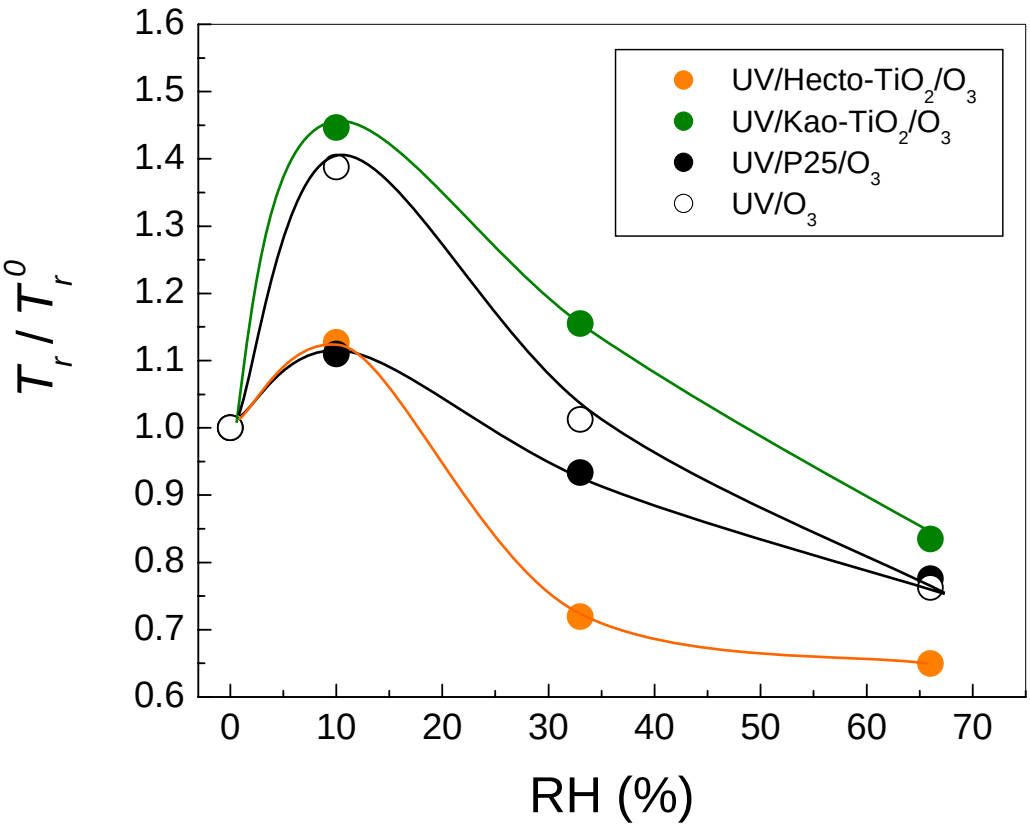

Figure 3: Effect of relative humidity (RH) on the relative enhancement (T_r/T_r^0 >1) or inhibition (T_r/T_r^0 < 1) of the toluene removal rate with respect to dry air conditions.

Structural imperatives to improve elimination of hydrophobic VOCs using clay-TiO_2 composite photocatalysts

Clay-TiO_2 composites such as those evaluated in this study present some structural and physico-chemical characteristics that could be potentially advantageous for the photocatalytic removal of air pollutants. In these materials, anatase nanoparticles are embedded in the structure of porous clays, thus avoiding macroscopic aggregates of photoactive particles that may lead to reduced efficiency. Furthermore, clays are stable supports that protect the TiO_2 particles from erosion or washing. In our experiments under UVC irradiation, in which O_3 and short-lived reactive species were present, contact with the clay structure was shown either not to quench the oxidation process (Hecto-TiO_2), or to exhibit a positive synergy leading to an enhanced toluene removal (Kao-TiO_2).

However, the efficiency of clay-TiO_2 composite photocatalysts can be affected by several factors. On a catalyst mass basis, the samples considered in this study did not perform at the same level or better than P25. Relative humidity affected differently each of the two clay-TiO_2 samples, being relatively favorable for Kao-TiO_2 but very negative for Hecto-TiO_2, compared to the effect observed for P25. Since indoor air cleaners operate typically under moderate RH conditions, the reduced efficacy observed in the presence of moisture is a critical parameter to be considered in order to design photocatalysts that can eliminate hydrophobic VOCs. The effect of co-adsorbed water on the photocatalytic removal of one VOC (toluene) over different photocatalysts (P25, Hecto-TiO_2, Kao-TiO_2) reported here is consistent with our previous observations comparing a mixture of several VOCs of different hydrophilicity on the same photocatalytic surface *(4)*. In both cases, our results suggest that competition of VOCs with an excess of water on the surface of the catalyst is an important factor affecting overall conversion. For Hecto-TiO_2, even when the composite synthesis successfully increased the (already large) available surface area in the clay for VOC adsorption through incorporation of a large amount of titania, water adsorption and condensation on the pores may severely limit its effectiveness in the elimination of hydrophobic VOCs. Hence, clay materials combining high surface area and porosity (such as hectorite) with relatively less hydrophilic surfaces (such as kaolinite) should be a more effective photocatalyst for the elimination of hydrophobic VOCs. The effectiveness of

UVPCO air cleaners coated with P25 or other pure TiO_2 particles is limited by the relatively low conversion efficiency of alkanes, alkenes and aromatic hydrocarbons. For that reason, replacing conventional photocatalysts with porous, relatively less polar clay-TiO_2 composites has the potential for significantly improving the performance of photocatalytic air cleaners.

Acknowledgements

The authors express gratitude to R. Maddalena (LBNL) for GC/MS support, to L.A. Gundel and R. Dod (LBNL) for helpful discussions, and to M. Trejo (UNAM) for his participation in the synthesis of composite materials. Experimental work was carried out at LBNL under US DOE Contract No. DE-AC02-05CH11231.This project was supported in part by LBNL (LDRD LB07014, Project # 366088), by UNAM (PAPIIT Grant No: IN116007-2) and by CONACYT (SEP-CONACYT Ciencia Básica 2006, Grant nr. 61670). DK thanks the support of a DGAPA-UNAM scholarship. JCS thanks the support of the Mexican Academy of Sciences (Academia Mexicana de Ciencias) and The United States-Mexico Foundation for Science (Fundación México-Estados Unidos para la Ciencia) through the 2006-Young Researcher Summer Program Fellowship (AMC-FUMEC).

Supporting Information Available

Additional description of experimental methods, experimental results and figures describing the bench-scale flow reactor and typical experimental results are provided. The information is available free of charge via the Internet at http://pubs.acs.org

Literature cited

(1) Hoffmann, M. R.; Martin, S. T.; Choi, W.; Bahnemann, D. W. Environmental applications of semiconductor photocatalysis *Chem. Rev.* **1995**, *95*, 69-96.

(2) Pichat, P.; Disdier, J.; Hoang-van, C.; Mas, D.; Goutailler, G.; Gaysse, C. Purification/deodorization of indoor air and gaseous effluents by TiO_2 photocatalysis *Catalysis Today* **2000**, *63*, 363-369.

(3) Ollis, D. F. Photocatalytic purification and remediation of contaminated air and water *Comptes Rendues Acad. Sci. Paris - Chemistry* **2000**, *3*, 405-411.

(4) Hodgson, A. T.; Destaillats, H.; Sullivan, D.; Fisk, W. J. Performance of ultraviolet photocatalytic oxidation for indoor air cleaning applications *Indoor Air* **2007**, *17*, 305-316.

(5) Salthammer, T.; Fuhrmann, F. Photocatalytic surface reactions on indoor wall paint *Environ. Sci. Technol.* **2007**, *41*, 6573-6578.

(6) Auvinen, J.; Wirtanen, L. The influence of photocatalytic interior paints on indoor air quality *Atmos. Environ.* **2008**, *42*, 4101-4112.

(7) Strini, A.; Cassese, S.; Schiavi, L. Measurement of benzene, toluene, ethylbenzene and o-xylene gas phase photodegradation by titanium dioxide dispersed in cementitious materials using a mixed flow reactor *Appl. Catalysis B - Environmental* **2005**, *61*, 90-97.

(8) Puzenat, E.; Pichat, P. Studying TiO_2 coating on silica-covered glass by O2 photosorption measurements and FTIR-ATR spectrometry. Correlation with the self-cleaning efficacy *J. Photochem. Photobiol. A: Chemistry* **2003**, *160*, 127-133.

(9) Horikoshi, S.; Watanabe, N.; Onishi, H.; Hidaka, H.; Serpone, N. Photodecomposition of a nonylphenol polyethoxylate surfactant in a cylindrical photoreactor with TiO_2 immobilized fiberglass cloth *Appl. Catalysis B - Environmental* **2002**, *37*, 117-129.

(10) Raillard, C.; Hequet, V.; Le Cloirec, P.; Legrand, J. Photocatalytic oxidation of methyl ethyl ketone over sol-gel and commercial TiO_2 for the improvement of indoor air *Water Sci. and Technol.* **2006**, *53*, 107-115.

(11) Herrmann, J. M.; Tahiri, H.; Guillard, C.; Pichat, P. Photocatalytic degradation of aqueous hydroxy-butandioic acid (malic acid) in contact with powdered and supported titania in water *Catalysis Today* **1999**, *54*, 131-141.

(12) Raillard, C.; Hequet, V.; Le Cloirec, P.; Legrand, J. Kinetic study of ketones photocatalytic oxidation in gas phase using TiO_2-containing paper: effect of water vapor *J. Photochem. Photobiol. A: Chemistry* **2004**, *163*, 425-431.

(13) Guo, T.; Bai, Z.; Wu, C.; Zhu, T. Influence of relative humidity on the photocatalytic oxidation (PCO) of toluene by TiO_2 loaded on activated carbon fibers: PCO rate and intermediates accumulation *Appl. Catalysis B - Environmental* **2008**, *79*, 171-178.

(14) Keller, N.; Rebmann, G.; Barraud, E.; Zahraa, O.; Keller, V. Macroscopic carbon nanofibers for use as photocatalyst support *Catalysis Today* **2005**, *101*, 323-329.

(15) Xie, T.-H.; Lin, J. Origin of photocatalytic deactivation of TiO_2 film coated on ceramic substrate *J. Phys.Chem. C* **2007**, *111*, 9968-9974.

(16) Teekateerawej, S.; Nishino, J.; Nosaka, Y. Design and evaluation of photocatalytic micro-channel reactors using TiO_2-coated porous ceramics *J. Photochem. Photobiol. A: Chemistry* **2006**, *179*, 263-268.

(17) Chen, Y. J.; Dionysiou, D. D. Correlation of structural properties and film thickness to photocatalytic activity of thick TiO_2 films coated on stainless steel *Appl. Catalysis B - Environmental* **2006**, *69*, 24-33.

(18) Sanchez, B.; Coronado, J. M.; Candal, R.; Portela, R.; Tejedor-Tejedor, I.; Anderson, M. A.; Tompkins, D. T.; Lee, T. Preparation of TiO_2 coatings on PET monoliths for the photocatalytic elimination of trichloroethylene in the gas phase *Appl. Catalysis B - Environmental* **2006**, *66*, 295-301.

(19) Portela, R.; Sanchez, B.; Coronado, J. M.; Candal, R.; Suarez, S. Selection of TiO_2-support: UV-transparent alternatives and long-term use limitations for H2S removal *Catalysis Today* **2007**, *129*, 223-230.

(20) Sakatani, Y.; Grosso, D.; Nicole, L.; Boissiere, C.; Soler-Illia, G. J. A. A.; Sanchez, C. Optimised photocatalytic activity of grid-like mesoporous TiO_2 films: effect of crystallinity, pore size distribution and pore accessibility *J. Mater. Chem.* **2006**, *16*, 77-82.

(21) Thompson, T. L.; Yates, J. T. Surface science studies of the photoactivation of TiO_2-new photochemical processes *Chem. Rev.* **2006**, *106*, 4428-4453.

(22) Chen, X.; Mao, S. S. Titanium dioxide nanomaterials: synthesis, properties, modifications and applications. *Chem. Rev.* **2007**, *107*, 2891-2959.

(23) Litter, M. I.; Navio, J. A. Photocatalytic properties of iron-doped titania semiconductors *J. Photochem. Photobiol. A: Chemistry* **1996**, *98*, 171-181.

(24) In, S.; Orlov, A.; Berg, R.; Garcia, F.; Pedrosa-Jimenez, S.; Tikhov, M. S.; Wright, D. S.; Lambert, R. M. Effective visible light-activated B-doped and B,N-codoped TiO_2 photocatalysts *J. Amer. Chem. Soc.* **2007**, *129*, 13790.

(25) Chen, Y.; Crittenden, J. C.; Hackney, S.; Sutter, L.; Hand, D. W. Preparation of a novel TiO_2-based *p-n* junction nanotube photocatalyst *Environ. Sci. Technol.* **2005**, *39*, 1201-1208.

(26) Pichat, P.; Khalaf, H.; Tabet, D.; Houari, M.; Saidi, M. Ti-montmorillonite as photocatalyst to remove 4-chlorophenol in water and methanol in air *Environ. Chem. Lett.* **2005**, *2*, 191-194.

(27) Kun, R.; Mogyorosi, K.; Dekany, I. Synthesis and structural and photocatalytic properties of TiO_2/montmorillonite nanocomposites *Appl. Clay Sci.* **2006**, *32*, 99-110.

(28) Ooka, C.; Yoshida, H.; Suzuki, K.; Hattori, T. Effect of surface hydrophobicity of TiO_2-pillared clay on adsorption and photocatalysis of gaseous molecules in air *Appl. Catalysis A: General* **2004**, *260*, 47-53.

(29) Mogyorosi, K.; Dekany, I.; Fendler, J. H. Preparation and characterization of clay mineral intercalated titanium dioxide nanoparticles *Langmuir* **2003**, *19*, 2938-2946.

(30) Mogyorosi, K.; Farkas, A.; Dekany, I.; Ilisz, I.; Dombi, A. TiO_2 based photocatalytic degradation of 2-chlorophenol adsorbed on hydrophobic clay *Environ. Sci. Technol.* **2002**, *36*, 3618-3624.

(31) Morrissey, F. A.; Grismer, M. E. Kinetics of volatile organic compound sorption/desorption on clay minerals *J. Contam. Hydrol.* **1999**, *36*, 291-312.

(32) Solomon, D. Clay minerals as electron acceptors and/or donors in organic reactions *Clays and Clay Minerals* **1968**, *16*, 31-39.

(33) Mingelgrin, U.; Saltzman, S. Surface reactions of parathion on clays *Clays and Clay Minerals* **1979**, *27*, 72-78.

(34) Fusi, P.; Ristori, G.; Franci, M. Adsorption and catalytic decomposition of 4-nitrobenzene sulphonylmethylcarbamate by smectite *Clays and Clay Minerals* **1982**, *30*, 306-310.

(35) Ernstsen, V. Reduction of nitrate by Fe^{2+} in clay minerals *Clays and Clay Minerals* **1996**, *44*, 599-608.

(36) Kibanova, D.; Trejo, M.; Destaillats, H.; Cervini-Silva, J. Synthesis of hectorite-TiO_2 and kaolinite-TiO_2 nanocomposites with photocatalytic activity for the degradation of model air pollutants *Applied Clay Science* **2009**, *42,* 563-568.

(37) Jeong, J.; Sekiguchi, K.; Lee, W.; Sakamoto, K. Photodegradation of gaseous volatile organic compounds (VOCs) using TiO_2 photoirradiated by an ozone-producing UV lamp: decomposition characteristics, identification of by-products and

water-soluble organic intermediates *J. Photochem. Photobiol. A: Chemistry* **2005**, *169*, 279-287.

(38) Jeong, J.; Sekiguchi, K.; Sakamoto, K. Photochemical and photocatalytic degradation of gaseous toluene using short-wavelength UV irradiation with TIO_2 catalyst: comparison of three UV sources *Chemosphere* **2004**, *57*, 663-671.

(39) Yu, K.-P.; Lee, G. W. M. Decomposition of gas-phase toluene by the combination of ozone and photocatalytic oxidation process (TiO_2/UV, TiO_2/UV/O_3, and UV/O_3) *Appl. Catalysis B - Environmental* **2007**, *75*, 29-38.

(40) Wang, W.; Chiang, L.-W.; Ku, Y. Decomposition of benzene in air streams by UV/TiO_2 process *J. Hazardous Mat.* **2003**, *B101*, 133-146.

(41) Luo, Y.; Ollis, D. F. Heterogeneous photocatalytic oxidation of trichloroethylene and toluene mixtures in air: kinetic promotion and inhibition, time-dependent catalyst activity *J. of Catalysis* **1996**, *163*, 1-11.

(42) Sleiman, M.; Conchon, P.; Ferronato, C.; Chovelon, J.-M. Photocatalytic oxidation of toluene at indoor air levels (ppbv): towards a better assessment of conversion, reaction intermediates and mineralization *Appl. Catalysis B - Environmental* **2008**, *in press*.

(43) Singer, B. C.; Hodgson, A. T.; Destaillats, H.; Hotchi, T.; Revzan, K. L.; Sextro, R. G. Indoor sorption of surrogates for sarin and related nerve agents *Environ. Sci. Technol.* **2005**, *39*, 3203-3214.

(44) D'hennezel, O.; Pichat, P.; Ollis, D. F. Benzene and toluene gas-phase photocatalytic degradation over H_2O and HCl pretreated TiO_2: by-products and mechanisms. *J. Photochem. Photobiol. A: Chemistry* **1998**, *118*, 197-204.

(45) Blount, M. C.; Falconer, J. L. Characterization of adsorbed species on TiO_2 after photocatalytic oxidation of toluene *J. of Catalysis* **2001**, *200*, 21-33.

(46) Blount, M. C.; Falconer, J. L. Steady-state surface species during toluene photocatalysis *Appl. Catalysis B: Environmental* **2002**, *39*, 39-50.

(47) Hodgson, A. T.; Levin, H. "Volatile organic compounds in indoor air: a review of concentrations measured in North America since 1990," Lawrence Berkeley National Laboratory, 2003. (eetd.lbl.gov/IE/pdf/LBNL-51715.pdf)

(48) Destaillats, H.; Maddalena, R. L.; Singer, B. C.; Hodgson, A. T.; McKone, T. E. Indoor pollutants emitted by office equipment: a review of reported data and information needs *Atmos. Environ.* **2008**, *42*, 1371-1388.

(49) Mermut, A. R.; Cano, A. F. Baseline studies of the Clay Minerals Society Source Clays: chemical analysis of major elements *Clays and Clay Minerals* **2001**, *49*, 381-386.

(50) USEPA "Method TO-1, Revision 1,0: Method for the determination of volatile organic compounds in ambient air using Tenax(R) Adsorption and gas chromatography/mass spectrometry (GC/MS)," Center for Environmental Research Information, Office of Research and Development US Environmental Protection Agency, 1984.

(51) Toby, S.; Van der Burgt, L. J.; Toby, F. S. Kinetics and chemiluminescence of ozone aromatic reactions in the gas phase *J. Phys. Chem.* **1985**, *89*, 1982-1986.

(52) Cvetanovic, R. J. Evaluated chemical kinetic data for the reactions of atomic oxygen O(P-3) with unsaturated hydrocarbons *J. Phys. Chem. Ref. Data* **1987**, *16*, 261-326.

(53) Atkinson, R.; Aschmann, S. M. Rate constants for the gas phase reactions of the OH radical with a series of aromatic hydrocarbons at 296 +/- 2 K *Int. J. Chem. Kinetics* **1989**, *21*, 355-365.

(54) Obee, T. N.; Brown, R. T. TiO_2 photocatalysis for indoor air applications: effects of humidity and trace contaminant levels on the oxidation rates of formaldehyde, toluene and 1,3-butadiene *Environ. Sci. Technol.* **1995**, *29*, 1223-1231.

(55) Pengyi, Z.; Fuyan, L.; Gang, Y.; Qing, C.; Wanpeng, Z. A comparative study on decomposition of gaseous toluene by O_3/UV, TiO_2/UV and O_3/TiO_2/UV *J. Photochem. Photobiol. A: Chemistry* **2003**, *156*, 189-194.

BRIEF

The performance of novel hectorite-TiO_2 and kaolinite-TiO_2 photocatalysts is evaluated by following the removal of realistically low toluene concentrations from dry and humidified air.